

GREY TONE LEVEL IMAGES CHARACTERIZATION BY MORPHOLOGICAL
FUNCTIONS : APPLICATION TO NON PLANAR SURFACES

Gervais GAUTHIER, Jacques-Olivier REBILLON, Michel COSTER,
Eric HÉNAULT

Laboratoire d'Etudes et de Recherches sur les Matériaux, LERMAT URA CNRS
n° 1317, ISMRA, 6, Boulevard du Maréchal Juin, 14050 CAEN Cedex, FRANCE

ABSTRACT

A few notions about the surface area and the surface roughness are reminded. Afterwards, a new expression of the surface roughness is introduced : the relative roughness. This is the expression of transformation of which an example is presented. This method is tested on fractal simulations and next, is applied to non planar surfaces.

Keywords : fractals, image analysis, Minkowski dimension, morphological transformations, non planar surfaces, roughness.

CALCULATION OF THE SURFACE AREA

The calculation of the surface area can be made with several methods. Hénault has described in his thesis (1992) three methods among these adapted to the image analysis : the method of triangulation, the stereological method based on the Crofton formula and the method generalizing the Steiner formula. This latest is adapted to the investigations using the concept of the fractal analysis. The expression of the generalized Steiner formula for a surface area is

$$S(f) = \lim_{r \rightarrow 0} \frac{V(SG(f) \oplus B(r)) - V(SG(f) \ominus \check{B}(r))}{2r} \quad [1]$$

where f is the function representing the non planar surface and $SG(f)$ is its subgraph, $B(r)$ is the ball of radius r and $S(f)$ is the surface area of f calculated in \mathbb{R}^3 .

SURFACE ROUGHNESS R_A

The surface area is an absolute parameter and our images are known solely in a mask so it is necessary to use a relative parameter : the surface roughness, noted R_A . It is defined by the following expression :

$$R_A = \frac{S(f)}{A(\text{supp}(f))} \quad [2]$$

in which $\text{supp}(f)$ is the support of f (mask of the image).

This definition of the roughness is commonly the most embraced in quantitative fractography (Kendall and Moran, 1963; El Soudani, 1974; Chermant and Coster, 1979). Nevertheless, it is not adapted to the images acquired in the SEM, because it depends on the anamorphosis (Hénault, 1992; Coster, 1992) hence on the conditions of acquisition. Therefore, our aim is to find a new definition of the roughness adapted to all the means of acquisition.

INTRODUCTION OF THE RELATIVE ROUGHNESS

Then we must approach the roughness in a different way. Numerous authors have studied the non planar surfaces by the fractal models (Coster and Deschanvres, 1978; Underwood and Banerji, 1986; Baran et al., 1992). We take back this idea in which measurement of the surface area corresponds to an overlapping of this by a volumic structuring element. The difference between the dilated and eroded of the image, or the subgraph of f , is a compatible transformation with that. The axis z (photometric axis) has not the same scale as another axis (spacial axis) then the hypothesis of self-similarity used in fractal analysis is not verified in this case. On the other hand, we can test the validity of the hypothesis of self-affinity and calculate the fractal dimension with the method of Minkowski-Bouligand which is defined for a curve by :

$$D_M(f) = \lim_{\lambda \rightarrow 0} (2 - \log(S_2(f, \lambda)) / \log(2\lambda)) \tag{3}$$

with $S_2(f, \lambda)$ being the surface area of the Minkowski ribbon obtained by dilation of the function f , representing the curve \mathcal{L} , by the disk of radius λ (figure 1).

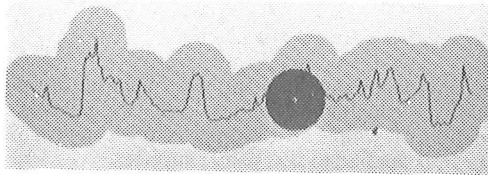


Figure 1 : curve \mathcal{L} (—) and its dilation (■) by a disk of radius λ (●).

Likewise, the Minkowski dimension for a surface \mathcal{S} is defined by :

$$D_M(f) = \lim_{\lambda \rightarrow 0} (3 - \log(V(f, \lambda)) / \log(2\lambda)) \tag{4}$$

with $V(f, \lambda)$, the volume obtained by dilation of the function f , representing the surface \mathcal{S} , by the ball of radius λ .

In the same way, we can study a function called function of relative roughness. It is defined by the next expression :

$$R_s(f, \lambda) = S(f, \lambda) / S(f, \lambda_0) \tag{5}$$

where λ is the current step of measurement and λ_0 is the shortest step.

The division of the surface area $S(f, \lambda)$ by a surface area $S(f, \lambda_0)$ reduces the influence of the anamorphosis. Only the transformation depends on it. If the flat structuring element is employed then the measurement is independent of the anamorphosis. Contrary to the classical roughness, the relative roughness has a meaning exclusively when the transformation is performed, because it is the expression of this transformation.

USE OF THE STEINER'S METHOD

The volume calculated in the relation [4] can be expressed by :

$$V(f, \lambda) = V(SG(f) \oplus \lambda B) - V(SG(f) \ominus \lambda \check{B}) \tag{6}$$

where B is a ball with a unit radius.

The generalization of the Steiner's formula to any radius λ is :

$$S(f, \lambda) = \frac{V(SG(f) \oplus \lambda B) - V(SG(f) \ominus \lambda \check{B})}{2\lambda} \tag{7}$$

Thus the relation [4] becomes :

$$D_M(f) = \lim_{\lambda \rightarrow 0} (2 - \log(S(f, \lambda)) / \log(2\lambda)) \tag{8}$$

The study of $\log(S(f, \lambda))$ versus $\log(2\lambda)$ will allow to assert or to invalidate the hypothesis of self-affinity, and, in all case, to know the instantaneous dimension of the surface for λ (similarity ratio).

APPLICATIONS

i) Analysed images

This method is tested on simulations and real non planar surfaces like the surfaces of fracture (steel, alumina) and ground samples. The large variety of textures of these images allows to verify the general sight of the method.

ii) Structuring elements

In the expression [7], B is a ball but another structuring element can be used. In fact, the method based on the Steiner formula is tested with the following structuring elements : the rhombododecahedron, the cuboctahedron, the pyramid with a square base and the cube for the volumic elements, and the squared flat structuring element.

The divergence between the curves $\log(R_s(f, \lambda))$ versus $\log(2\lambda)$ for the different structuring elements increases with λ (figure 3). The limit of this curve when λ tends towards the infinity depends on the structuring element. The slope of the asymptote is null for the volumic elements and -1 for the flat elements. When λ is not negligible in comparison with the size of the support of f , this slope has no meaning for the flat element because it implies an instantaneous dimension equal to 3, whereas a surface without overlapping can not reach this dimension. For the volumic element, the instantaneous dimension is equal to 2 that corresponds to a surface viewed without relief by an element of great size. In this two cases, we restrict the study of $\log(S(f, \lambda))$ to the small values of λ faced with the size of the support.

In this conditions, each structuring element acts differently and allows to apprehend the geometry of the relief. However the anamorphosis modifies the intensity of the relief and all volumic structuring elements are sensitive to this (figure 2.a). Only the flat structuring element is independent of the anamorphosis (figure 2.b) and can verify the hypothesis of self-affinity.

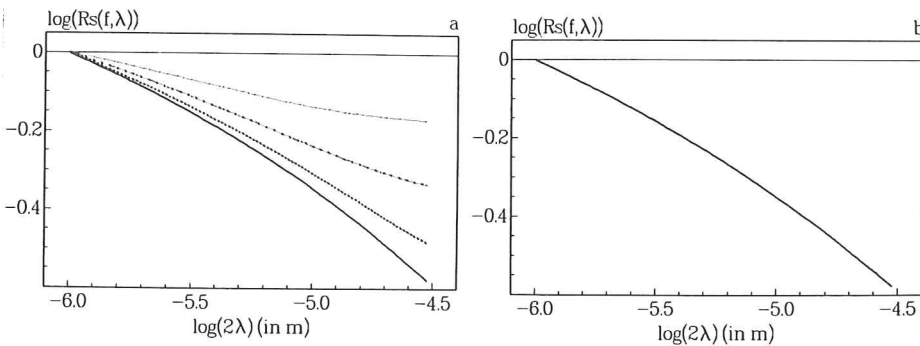


Figure 2 : Linear anamorphosis (divided by 1 (—), 2 (---), 4 (-.-.-) and 8 (.....)) on images of fracture of alumina C for a magnification 500 studied by a volumic structuring element (a) (rhombododecahedron) and by a flat structuring element (b).

iii) Influence of the parameters of acquisition

The photometric differences between two points of the image can not be linked up to the

difference of its real heights on the observed surface when the observation is effected on the SEM. The variation of each parameter of the SEM leads to an anamorphosis of the surface. The modifications of the parameters imply the different results when a volumic structuring element is used. On the other hand, the results are stable when a flat structuring element is employed and the variation of the parameters does not bring about a saturation of the image (the grey tone levels must be over 0 and under 255 for a 8-bits image).

iv) Test of the method on fractal simulations

The simulations (figure 3) that we have employed are created by an algorithm based on the midpoint displacement (Barnsley et al., 1988). afterwards, they undergo a linear anamorphosis on the photometric values so that the grey tone levels are spread between 0 and 255.

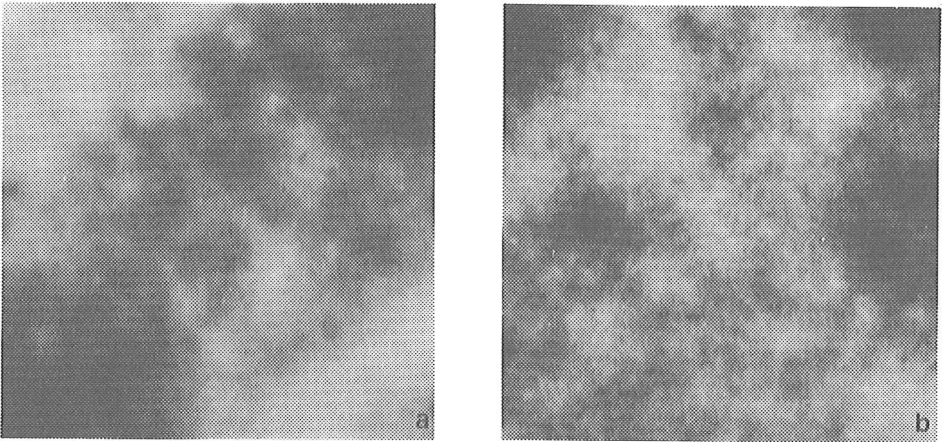


Figure 3 : simulations of fractal surfaces of which dimensions are 2.3 (a) and 2.5 (b).

Several images have been constructed with different dimensions and tested by the method described above. The curves $\log(Rs(f,\lambda))$ versus $\log(2\lambda)$ are not rectilinear and varies in function of the structuring element (figure 4).

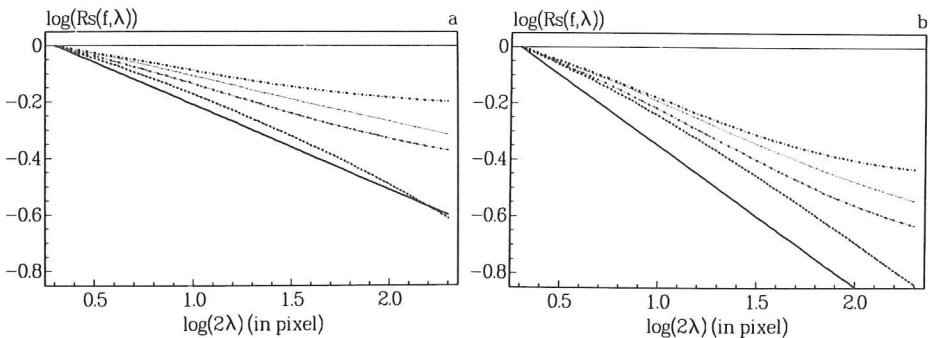


Figure 4 : $\log(Rs(f,\lambda))$ versus $\log(2\lambda)$ by the flat structuring element (—), the pyramid (- · - ·), the cuboctahedron (.....) and the rhombododecahedron (- - -) on the fractal simulations of which dimension is 2.3 (a) and 2.5 (b). The theoretical curve is represented by (—).

In all the cases, the calculated dimension increases with the implanted dimension (figure 5). This interesting result allows a comparative study of the roughness of images, without measuring in z-axis when the transformation by the flat structuring element is used. The hypothesis of the self-affinity cannot be verified nevertheless we can quantify the roughness.

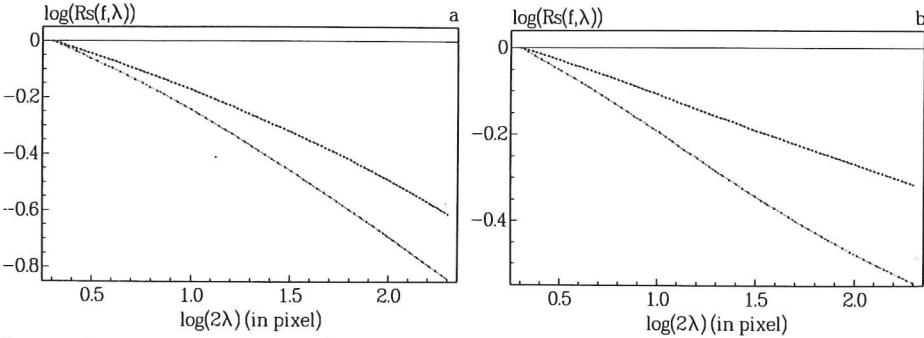


Figure 5 : $\log(Rs(f,\lambda))$ versus $\log(2\lambda)$ by the flat structuring elements (a) and the cuboctahedron (b) on the fractal simulations of which dimension is 2.3 (---) and 2.5 (....).

v) Application to the non planar surfaces

Several surfaces have been studied (figure 6). The curves $\log(Rs(f,\lambda))$ versus $\log(2\lambda)$ are not lines (figure 7). In fact, the analysed surfaces are not fractal surfaces yet the notion of instantaneous dimension is interesting to study the roughness for a fixed magnification.

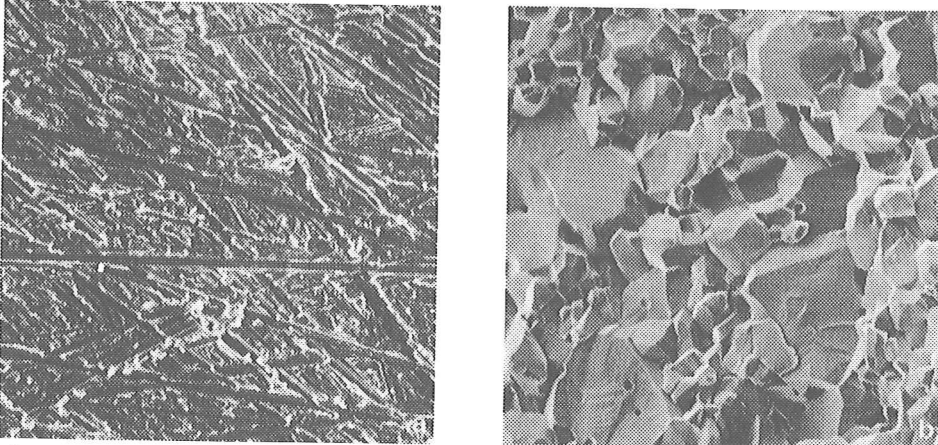


Figure 6 : ground aluminium alloy for a magnification 350 (a); fracture surface of alumina C for a magnification 750 (b).

The method presented in this paper allows to use the SEM to classify the surfaces by its roughness with the instantaneous dimension.

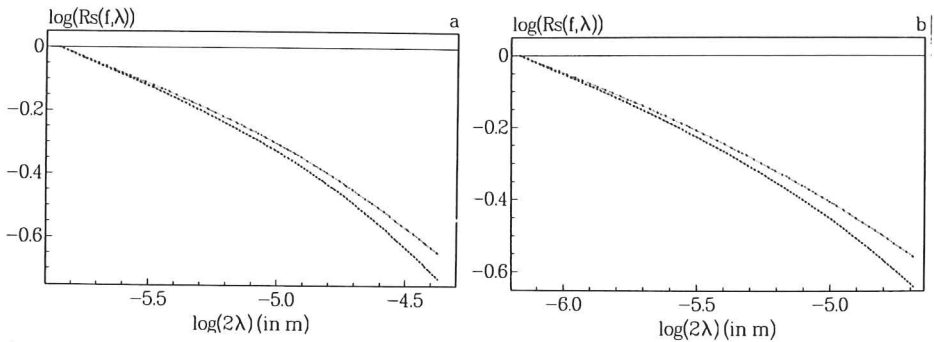


Figure 7 : $\log(Rs(f, \lambda))$ versus $\log(2\lambda)$ with the flat structuring element (---) and with the cuboctahedron (....) on the surface of ground aluminium alloy (a) and on the fracture surface of alumina C.

CONCLUSION

We have showed that the surfaces can be classified in function of their roughness by the instantaneous dimension calculated by the described method with a fixed structuring element and a fixed magnification. In addition, the influence of the intrinsic anamorphosis of the SEM on the measurement has been removed using flat structuring element.

REFERENCES

- Baran GR, Rocques-Carmes C, Wehbi D, Degrange M. Fractal characteristics of fracture surfaces. *J Am Ceram Soc* 1992; **75** : 2687-91.
- Barnsley MF, Devaney RL, Mandelbrot BB, Peitgen H-O, Saupe D, Voss RF. *The science of fractal images*. Berlin : Springer-Verlag 1988; 95-105.
- Chermant JL, Coster M. Quantitative fractography. *J Mat Sci* 1979; **14** : 509-534.
- Coster M, Deschanvres A. Fracture, objet fractal et morphologie mathématique. *Pract Met* 1978; **8S** : 61-73.
- Coster M. Morphological tools for non planar surfaces analysis. *Acta Stereol* 1992; **11** Suppl 1 : 639-650.
- El Soudani SM. Theoretical basis for the quantitative analysis of fracture surfaces. *Metallography* 1974; **7** : 271-311.
- Hénault E. Caractérisation géométrique d'images en niveaux de gris : application à l'analyse des surfaces non planes. Thèse de Doctorat de l'Université de Caen, 1992.
- Kendall MG, Moran PAP. *Geometrical probability*. London : Charles Griffin 1963.
- Underwood EE, Banerji K. Fractals in fractography. *Materials Science and Engineering* 1986; **80** : 1-14.